REPORT DOCUMENTATION PAGE

Form Approved OMB NO. 0704-0188

1. REPORT DATE (DD-MM-YYYY)	2. REPORT TYPE	3. DATES COVERED (From - To)
	New Reprint	-

4. TITLE AND SUBTITLE

A high-performance lithium-ion battery anode based on the core–shell heterostructure of silicon-coated vertically aligned carbon nanofibers

5a. CONTRACT NUMBER	W911NF-12-1-0412
5b. GRANT NUMBER	
5c. PROGRAM ELEMENT NUMBER	611102
5d. PROJECT NUMBER	
5e. TASK NUMBER	
5f. WORK UNIT NUMBER	

6. AUTHORS

Ronald A. Rojeski, Brett A. Cruden, Jianwei Liu, Steven A. Klankowski, Judy Wu, Jun Li

7. PERFORMING ORGANIZATION NAMES AND ADDRESSES

University of Kansas Center for Research, Inc.
2385 Irving Hill Road

Lawrence, KS 66045 -7568

8. PERFORMING ORGANIZATION REPORT NUMBER

9. SPONSORING/MONITORING AGENCY NAME(S) AND ADDRESS(ES)

U.S. Army Research Office
P.O. Box 12211
Research Triangle Park, NC 27709-2211

10. SPONSOR/MONITOR'S ACRONYM(S)
ARO

11. SPONSOR/MONITOR'S REPORT NUMBER(S)
61858-EL.13

12. DISTRIBUTION AVAILIBILITY STATEMENT

Approved for public release; distribution is unlimited.

13. SUPPLEMENTARY NOTES

The views, opinions and/or findings contained in this report are those of the author(s) and should not contrued as an official Department of the Army position, policy or decision, unless so designated by other documentation.

14. ABSTRACT

This study reports a high-performance hybrid lithium-ion anode material based on coaxially coated Si shell on vertically aligned carbon nanofiber (VACNF) core. The unique cup-stacking-like graphitic microstructure of the VACNFs provides abundant broken graphitic edges at the sidewall, making VACNFs an interesting Li+ intercalation medium and, more importantly, a robust and highly conductive core which can form good interface with the active Si shell for Li+ storage. Reversible Li+ intercalation and extraction with the capacity of 350-400

15. SUBJECT TERMS

high-performance Li-ion battery anodes; nanostructured materials; silicon-carbon hybrid structure; vertically aligned carbon nanofibers; vertical core-shell nanowire arrays

16. SECURITY CLASSIFICATION OF:			17. LIMITATION OF ABSTRACT	15. NUMBER OF PAGES	19a. NAME OF RESPONSIBLE PERSON
a. REPORT	b. ABSTRACT	c. THIS PAGE			Judy Wu
UU	UU	UU	UU		19b. TELEPHONE NUMBER: 785-864-3240

Report Title

A high-performance lithium-ion battery anode based on the core–shell heterostructure of silicon-coated vertically aligned carbon nanofibers

ABSTRACT

This study reports a high-performance hybrid lithium-ion anode material based on coaxially coated Si shell on vertically aligned carbon nanofiber (VACNF) core. The unique cup-stacking-like graphitic microstructure of the VACNFs provides abundant broken graphitic edges at the sidewall, making VACNFs an interesting Li+ intercalation medium and, more importantly, a robust and highly conductive core which can form good interface with the active Si shell for Li+ storage. Reversible Li+ intercalation and extraction with the capacity of 350-400 mAhg-1 has been obtained with bare VACNFs at C/2 and C/1 rates. Upon sputtering deposition of Si, it forms an interesting core-shell vertical nanowire structure with a tapered coaxial Si shell. The uniform vertical alignment enables Si to spread along the whole VACNF length, resulting in a much smaller shell thickness. With the 10 ?m long VACNF arrays, the core-shell nanowires remain well separated from each other even after depositing a thick layer of Si equivalent to 1.5 ?m nominal thickness on flat substrates. This open three-dimensional hybrid architecture allows the Si shell to freely expand/contract in the radial direction during Li+2 insertion/extraction. High-performance lithium storage with the specific capacity of 3000-3650 mAhg-1 (normalized to the Si mass) has been achieved, which changes little as the power rate is increased by 20 times from C/10 to C/0.5 (or 2C). The obtained capacity matches the maximum reported value for amorphous Si, indicating that the Si shell is fully active due to effective charge collection by the VACNF core and short diffusion path for Li+ insertion/extraction. More importantly, ~89% of capacity is retained after charge-discharge for 100 cycles at C/1 rate. The ability to obtain high capacity at significantly improved power rates while maintaining the extraordinary cycle stability demonstrates that this novel structure is a very promising anode material for high-performance Li-ion batteries.

REPORT DOCUMENTATION PAGE (SF298)
(Continuation Sheet)

Continuation for Block 13

ARO Report Number 61858.13-EL
A high-performance lithium-ion battery anode ba ...

Block 13: Supplementary Note

Approved for public release; distribution is unlimited.

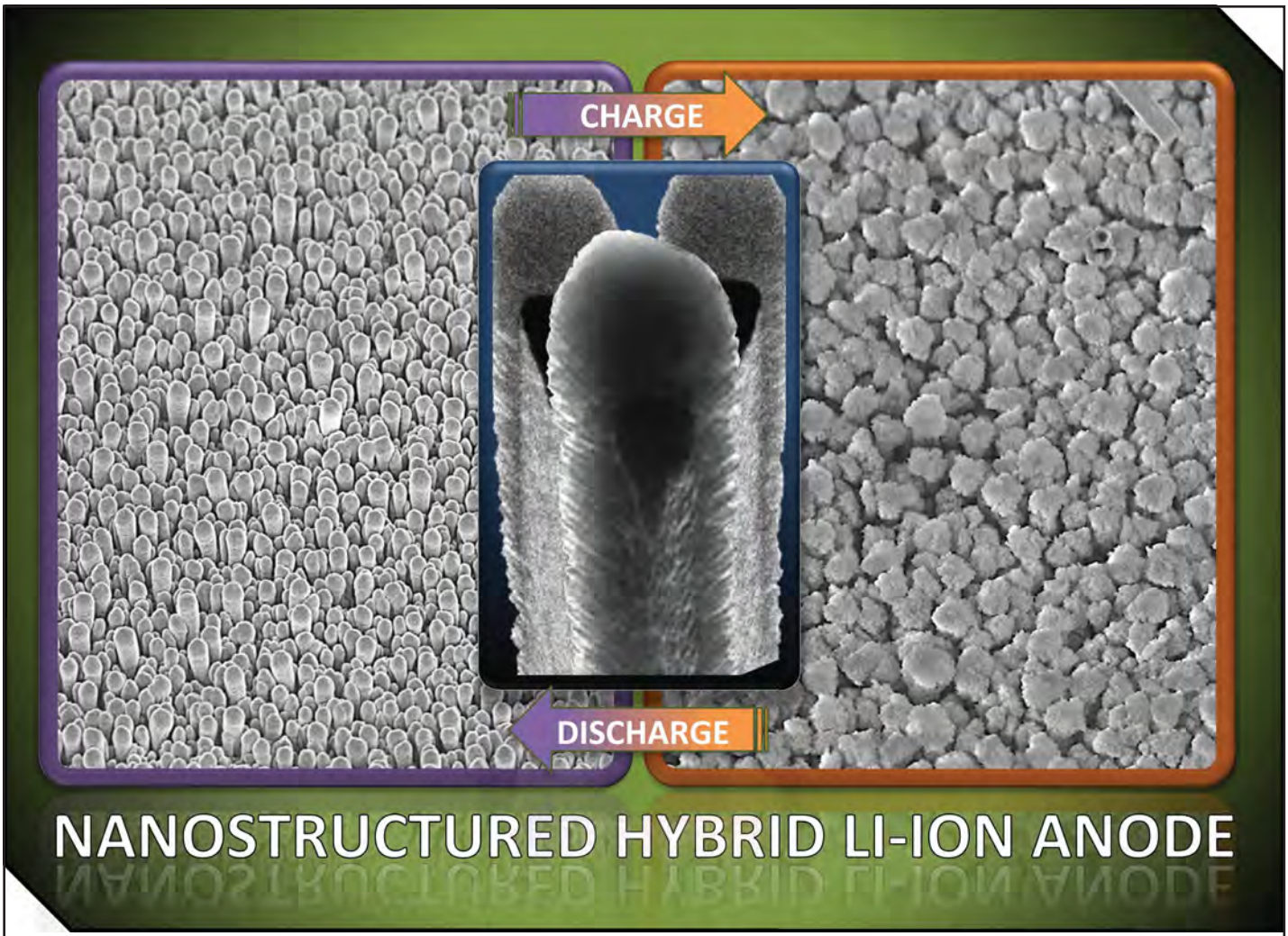

A university-industrial collaboration pushes forward development of novel Li-ion electrode materials, leveraging a partnership between the Nanomaterials Group of Prof. Jun Li at Kansas State University and Catalyst Power Technologies, a California based energy storage company.

Title: A high-performance lithium-ion battery anode based on the core–shell heterostructure of silicon-coated vertically aligned carbon nanofibers

This work introduces a unique hybrid anode for advanced Lithium-ion batteries. The core–shell architecture enables the silicon to radially expand and relieves stress upon lithium insertion while maintaining reliable and efficient electrical connection to the current collector through the carbon nanofibers. This novel architecture enables simultaneous high power density and high energy density for an anode in a lithium-ion battery.

As featured in:

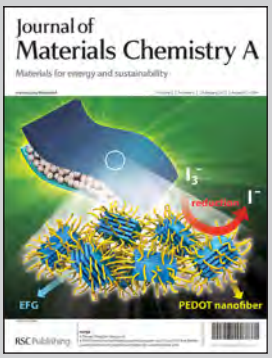

See S. A. Klankowski *et al.*, *J. Mater. Chem. A*, 2013, **1**, 1055.

RSC Publishing

www.rsc.org/MaterialsA

Registered Charity Number 207890

Journal of Materials Chemistry A

RSC Publishing

PAPER

View Article Online
View Journal | View Issue

Cite this: J. Mater. Chem. A, 2013, 1, 1055

A high-performance lithium-ion battery anode based on the core–shell heterostructure of silicon-coated vertically aligned carbon nanofibers†

Steven A. Klankowski,[a] Ronald A. Rojeski,[b] Brett A. Cruden,[c] Jianwei Liu,[d] Judy Wu[d] and Jun Li*[a]

Received 24th August 2012
Accepted 15th October 2012

DOI: 10.1039/c2ta00057a

www.rsc.org/MaterialsA

This study reports a high-performance hybrid lithium-ion anode material using coaxially coated silicon shells on vertically aligned carbon nanofiber (VACNF) cores. The unique "cup-stacking" graphitic microstructure makes VACNFs a good lithium-ion intercalation medium and, more importantly, a robust bush-like conductive core to effectively connect high-capacity silicon shells for lithium-ion storage. The vertical core–shell nanowires remain well separated from each other even after coating with bulk quantities of silicon (equivalent to 1.5 μm thick solid films). This open structure allows the silicon shells to freely expand/contract in the radial direction during lithium-ion insertion/extraction. A high specific capacity of 3000–3650 mA h $(g_{Si})^{-1}$, comparable to the maximum value of amorphous silicon, has been achieved. About 89% of the capacity is retained after 100 charge–discharge cycles at the C/1 rate. After long cycling, the electrode material becomes even more stable, showing the invariant lithium-ion storage capacity as the charge–discharge rate is increased by 20 times from C/10 to C/0.5 (or 2C). The ability to obtain high capacity at significantly improved power rates while maintaining the extraordinary cycle stability demonstrates that this novel structure could be a promising anode material for high-performance lithium-ion batteries.

Introduction

Rechargeable lithium ion batteries are key electrical energy storage devices for portable electronics, power tools, and future electric vehicles due to their high energy densities.[1,2] However, the obtainable energy capacity of today's commercial Li-ion batteries drops significantly as the charge–discharge rate is increased due to slow Li^+ transport in bulk host materials. Increasing energy density as well as the charging–discharging rate and cycle life is critical for broader applications of Li-ion batteries. Three-dimensional (3D) nanostructured electrode materials and architecture have been recognized as a promising pathway towards this goal due to the increased active surface area, shorter path length for Li^+ transport, and better accommodation of the strain accompanying the volume changes during lithium insertion/extraction.[3–7]

Most commercial Li-ion batteries employ graphite or other carbonaceous materials as anodes, which have a theoretical capacity limit at 372 mA h g^{-1} by forming a fully intercalated LiC_6 compound.[3] In contrast, crystalline silicon has a much higher theoretical specific capacity of 4200 mA h g^{-1} by forming fully lithiated alloy $Li_{4.4}Si$.[3] However, the volume expansion during Si lithiation as large as ~300% [8] causes great structural stress that inevitably leads to fractures and mechanical failure, which significantly limits the lifetime of Si anodes.[3,9] It is known that an ultrathin (≤50 nm) amorphous Si film can provide the highest capacity at ~3750 mA h g^{-1} and maintain this value for 200 cycles[10] but the small mass limits the attainable cell capacity. Increasing the Si film thickness for higher cell capacity has been explored but has been limited by rapid degradation in performance. As the Si film thickness was increased to ~250 nm, reversible capacity was only obtained at 3000 mA h g^{-1} for a few tens of cycles before declining considerably.[11,12]

A recent approach to addressing the mechanical strain in bulk and thin-film materials is by implementation of nanostructures with an enhanced surface-to-volume ratio that can accommodate the lattice stress. Indeed, improved mechanical stability and better electrical connection were obtained with Si nanowires (NWs) through reversible expansion/contraction in both radial and longitudinal directions.[9,13] A high capacity of ~3500 mA h g^{-1} was obtained over 20 charge–discharge cycles at a low charge–discharge rate of C/20,[9] where the rate notation

[a]Department of Chemistry, Kansas State University, Manhattan, KS 66506, USA. E-mail: junli@ksu.edu

[b]Catalyst Power Technologies, 200 Carlyn Avenue, Suite C, Campbell, CA 95008, USA. E-mail: rarojeski@gmail.com

[c]NASA Ames Center for Nanotechnology, Moffett Field, CA 94035, USA

[d]Department of Physics and Astronomy, The University of Kansas, Lawrence, KS 66045, USA

† Electronic supplementary information (ESI) available. See DOI: 10.1039/c2ta00057a

"C/*n*" represents applying a constant current with proper magnitude to charge/discharge the battery material to its full capacity over *n* hours. The magnitude of the current depends on the total capacity of the cell or the specific electrode. However, it dropped to ~2500 mA h g^{-1} or even lower as the rate was increased to C/2.[9] It is noted that the normal charge–discharge rate for commercial Li-ion batteries varies between C/5 and C/1, depending on the manufacturers. Therefore, the slow kinetics and the degradation in electrical connection still limited the available power density in the Si NW anode. Evidently, the resistivity of individual NWs was noted to increase by 150 times after lithiation.[9]

To maintain both structural integrity and electrical connection, it is necessary to employ hybrid structures with a stable core to support the active Li^+ storage materials. This was demonstrated by depositing Si shells or thick films on randomly stacked carbon nanofibers produced by conventional thermal pyrolysis.[14,15] As expected, the reversibility was significantly improved at C/5 or lower rates.[14] Over 98% coulombic efficiency was achieved in 55 charge–discharge cycles. However, the maximum capacity was only ~2000 mA h g^{-1} or even lower[14,15] at the C/5 rate and was only ~800 mA h g^{-1} at the C/1 rate (or referred to as the "1C" rate in some literature).[14] This was likely due to the non-uniform Si coating in these hybrid structures. Si tended to accumulate at the very top surface and did not penetrate deeply into the randomly arranged carbon nanofibers.[14,15] Such shadow effects can be resolved by using a vertically aligned nanofiber structure. Wang *et al.* explored depositing Si on vertically aligned multiwalled carbon nanotubes (MWCNTs) using chemical vapour deposition (CVD) to form a hybrid Si–MWCNT structure consisting of ~54 to 57 wt% of Si.[16] The initial specific capacity (normalized to Si mass) was as high as ~3300 mA h $(g_{Si})^{-1}$ at the ~C/19 rate. However, it dropped to ~1500 mA h $(g_{Si})^{-1}$ at the ~C/2 rate and retained less than 70% after 100 cycles.[16] The wavy and partially entangled structure may still have prevented uniform Si deposition deep into the MWCNT arrays. More uniformly aligned vertical NW arrays may be a better candidate for structural support, as demonstrated recently with straight Cu NW arrays.[17] This hybrid structure was able to retain 95% of the capacity after 35 cycles but the Si coating only presented ~25% of the theoretical capacity at the C/1 rate.[17] How to fully utilize this concept needs to be further explored.

Here we report another approach to fabricating hybrid core–shell NW architecture as a high-performance Li-ion anode by utilizing vertically aligned carbon nanofiber (VACNF) arrays on Cu foil to support coaxially coated silicon shells, as illustrated in Fig. 1. The VACNFs are a special type of MWCNTs which are grown with DC-biased plasma chemical vapour deposition (PECVD).[18–20] Due to the high electric field during growth, the VACNFs are aligned vertically on the substrate surface and remain well separated from each other, forming an untangled brush-like structure. The easily accessible open space from above allows Si to be coated onto each carbon nanofiber (CNF) to form rather uniform coaxial shells over the whole sample.

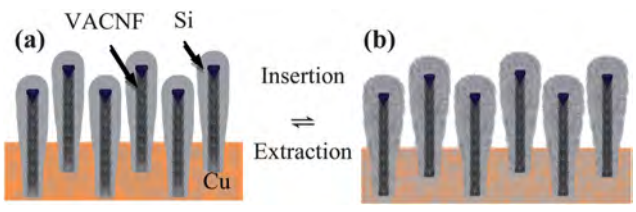

Fig. 1 Schematic illustration of the reversible structural changes of the coaxially coated Si on vertically aligned carbon nanofibers (VACNFs) in (a) extracted (discharged) and (b) inserted (charged) states during a half-cell test for Li-ion batteries.

Besides efficient electrical connection to the Si shell, this structure can effectively accommodate the volume expansion/contraction of Si in the radial direction during charge–discharge cycles. The short path of Li^+ transport across the thin Si shell should allow a much higher charge–discharge rate and significantly improved power density. In this work, we demonstrate that the Si material in this core–shell NW structure is fully active, providing high Li^+ storage capacity in the range of 3000 to 3650 mA h $(g_{Si})^{-1}$, even at a C/1 rate. Furthermore, the capacity is retained at this level for over 100 charge–discharge cycles. The charge–discharge rate, the corresponding capacity, and cycle stability are all significantly improved from previous reports on anode materials based on Si NWs and hybrid Si–C nanostructures.[9,14,15,21]

Experimental details

VACNF growth and Si deposition

Oxygen-free pure copper foils with a thickness of 84 μm and 12.7 μm, respectively, in the form of 29 cm wide long strips (Copper 102, Hamilton Precision Metals, PA) were employed, which were further cut into 15 cm × 29 cm sheets. After light cleaning of the copper sheets with chemical etching in 0.1% citric acid, a 300 nm thick chromium barrier layer followed by a 30 nm nickel catalyst layer was deposited using a high-vacuum Perkin Elmer 4400 series magnetron sputtering system at UHV Sputtering Inc. (Morgan Hill, CA). These Ni/Cr/Cu sheets were then cut into disks of 18 mm in diameter for half-cell tests.

VACNFs with average lengths of 3.0 μm and 10.0 μm, respectively, were grown on the Cu foils using a DC-biased PECVD system (AIXTRON, CA) following a procedure in the literature.[18,22,23] A pre-treatment procedure was applied first by thermally heating the Ni/Cr/Cu substrate to 500 °C in 250 sccm NH_3 at a pressure of 3.9 Torr and then applying plasma at 40 Watts for 60 seconds. The combined effects of thermal dewetting and NH_3 plasma etching broke down the Ni film into randomly distributed nanoparticles that catalysed the growth of VACNFs in a tip growth mode.[18,22,23] The diameter and distribution of the VACNFs were mostly determined by these Ni nanoparticles. After pre-treatment, a mixture of acetylene (at 70 sccm) and ammonia (at 250 sccm) was used as the precursors at 725 °C and a pressure of 4.6 Torr. The plasma power was kept at 45 Watts for 20 minutes to grow 3.0 μm long VACNFs and for 120 minutes to grow 10 μm long VACNFs, respectively. Pure silicon was deposited on VACNF arrays to form the VACNF-silicon core–shell nanowire arrays by high vacuum magnetron sputtering at UHV Sputtering Inc. The nominal thickness of Si (equivalent to the film thickness on a flat surface) was measured

in situ with a quartz microbalance (QCM) and validated by scanning electron microscopy (SEM) measurements of a silicon wafer placed beside the Cu substrate (see Fig. S1 in the ESI†).

Electrochemical cell assembly and charge–discharge tests

A reusable electrochemical cell (El-Cell, Hamburg Germany) with a three-electrode design was used for the half-cell tests. The Cu disks covered with VACNFs (with or without further Si coating) were used as the working electrode against an 18 mm dia. lithium disk (1.5 mm in thickness) as the counter electrode. A lithium wire was used as the reference electrode. A polyethylene spacer (0.65 mm in thickness) was placed between the working and counter electrodes. A Kelf ring (18 mm outer dia., 3.0 mm thick) with one side machined into a wedged shape was used to separate the working electrode from the polyethylene spacer so that the vertical nanowires were not compressed. The exposed working electrode area was 17.5 mm in diameter. The cell was assembled in an argon-filled dry-box (Mbraun LabStar50). The electrolyte consisted of 1.0 M lithium hexafluorophosphate ($LiPF_6$) in a mixture of a 1 : 1 : 1 volume ratio of ethylene carbonate (EC), ethyl methyl carbonate (EMC) and dimethyl carbonate (DMC) plus 2% vinylene carbonate (Novolyte, Ohio). Before testing, the electrolyte was injected by a syringe through a 0.30 mm dia. hole to fill between the electrodes. A small punch of pure lithium was then pressed into the hole to make direct contact with the electrolyte and served as the reference electrode. Cyclic voltammetry (CV) and galvanostatic charge–discharge cycles were performed using a PARStat 2273 potentiostat controlled by PowerSuite Software (Princeton Applied Research, Oak Ridge, TN), a CHI760D potentiostat controlled by CHI Electrochemical Software (CH Instruments, Austin, TX), and a MTI 8 channel battery analyser (MTI Corporation, Richmond, CA). Additional half-cell tests of the 10 μm long VACNF arrays were performed by cutting the 50.8 mm × 50.8 mm samples to an appropriate size for a 2032 button cell. CV and galvanostatic charge–discharge measurements of these samples were performed with an Arbin battery testing system (College Station, TX).

Microscopy and spectroscopy characterization

Both the as-prepared electrodes and those disassembled from the cells after Li-ion half-cell tests were stored and transferred in air before inspection with SEM (FEI Nano430). Some bare VACNFs and Si-coated VACNFs were scraped off from the Cu substrate, suspended in isopropanol by gentle stirring and then cast onto carbon film coated Cu grids for transmission electron microscopy (TEM) (FEI Tecnai F20 XT) measurements. Raman spectroscopy measurements were carried out with a Raman microscope (Thermo Scientific DXR system) with a 10× 0.25NA objective and a 532 nm laser at 5 mW power.

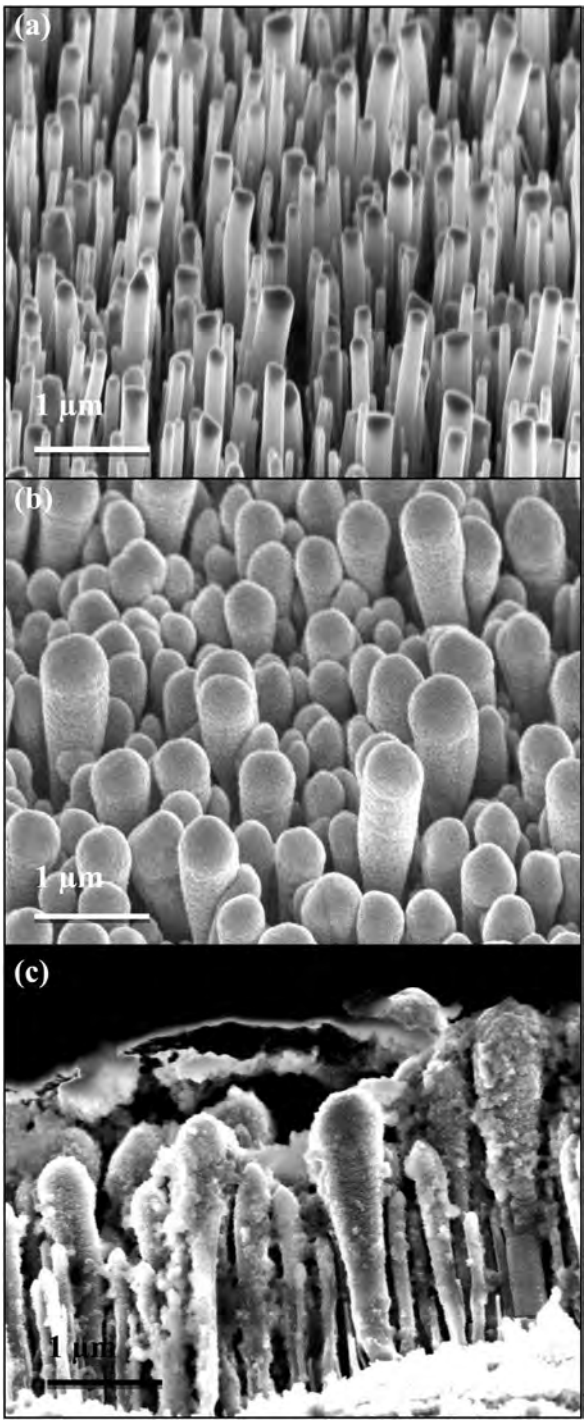

Fig. 2 SEM images of (a) an "as-grown" VACNF array with an average length of 3 μm, (b) a similar VACNF array after sputter-coating with silicon at a nominal thickness of 0.50 μm (*in situ* measured with a quartz crystal microbalance during deposition), and (c) the Si-coated VACNF array in the extracted (discharged) state after 100 charge–discharge cycles. Panels (a) and (b) are 45° perspective views and panel (c) is the cross-sectional view. All scale bars are 1.0 μm.

Results and discussion

Structural characterization of a Si-coated VACNF anode

Fig. 2 shows the SEM images of an "as-grown" VACNF array on a Cu foil, the VACNF array coated with a layer of Si, and the Si-coated VACNF array in the extracted (discharged) state after experiencing 100 lithium insertion–extraction (or charge–discharge) cycles, respectively. In the "as-grown" sample (Fig. 2a), CNFs were firmly attached to the Cu surface with a uniform vertical alignment. The distribution of CNF positions was random but overall the sample had a reproducible areal

density of 1.1×10^9 CNFs per cm^2 (counted with top-view SEM images). This translated to an average nearest-neighbour distance of ~330 nm. The average length of the CNFs in Fig. 2 was ~3.0 μm with >90% of CNFs in the range of 2.5 to 3.5 μm in length. The diameter spread from ~80 nm to 240 nm with an average of ~147 nm, as shown in the histogram in Fig. S2a†. An inverse teardrop shaped Ni catalyst particle for CNF growth is present at the tip of each CNF and caps the hollow central channel. The size of the Ni catalyst particle is known to define the diameter of the CNF.[18–20] In addition, it has been reported that nickel does not react with Li.[9]

After magnetron sputtering, it formed a thick Si coating at the VACNF tip and a gradually thinned coaxial Si shell moving down the CNF, presenting a tapered core–shell structure similar to a cotton swab. In this study, the total amount of Si deposited onto the VACNFs was represented by the nominal thickness equivalent to the Si films onto a flat surface, which was measured with a QCM and was further validated with cross-sectional SEM measurements of a Si wafer placed at the side of the Cu substrate during deposition. At 0.50 μm nominal thickness, the Si-coated VACNFs remained well-separated from each other, presenting an open core–shell NW array structure as shown in Fig. 2b, which allows the electrolyte to freely access the entire Si surface. The average tip diameter was ~457 nm, much bigger than the ~147 nm average diameter of "as-grown" VACNFs (see Fig. S2†). Thus the average radial Si thickness at the tip was estimated to be ~155 nm. This was apparently much smaller than the 0.50 μm nominal Si thickness since Si was spread along the full length of VACNFs. The cross-sectional SEM image in Fig. 2c clearly indicates that the Si shell covers the whole CNF length.

The TEM images in Fig. S3† and Fig. 3 further illustrate the detailed structure of the "as-grown" and Si-coated VACNFs before and after charge–discharge cycles as Li-ion anodes. As discussed earlier, these PECVD grown VACNFs have a unique interior microstructure distinct from the concentric tube structure of ordinary MWCNTs or the solid fibrous structure of pyrolyzed carbon nanofibers in other studies.[14,15] One of the most prominent characteristics is that these CNFs consist of a series of bamboo-like nodes across the mostly hollow central channel. The TEM image in Fig. S3a† indicates that these nodes consist of a stack of 5–15 cup-like graphitic layers, consistent with what has been reported in the literature.[18,19] The resolution and contrast were limited by the large CNF diameter (mostly between 100 and 200 nm in this study). The large diameter, however, is beneficial in ensuring that the CNFs are mechanically robust and able to retain the vertical array structure through Si deposition and wet electrochemical tests. The cup-stacking graphitic structure of the VACNF is schematically illustrated in Fig. S4.† The unique microstructure and brush-like configuration are key differences between this study and other nanostructured carbon materials in the literature.[14,15,21] It is noteworthy that the VACNF has relatively high electrical conductivity (up to $\sim 2.5 \times 10^5$ S m^{-1}) along the axis and is known to form a stable Ohmic contact with the conductive substrate.[24]

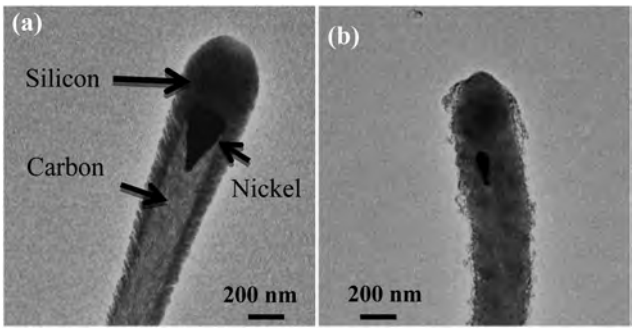

Fig. 3 Transmission electron microscopy images of (a) a VACNF coated with Si of 500 nm nominal thickness in the "as-prepared" state and (b) a VACNF in the delithiated (discharged) state after lithium insertion–extraction cycles. The CNFs were different ones randomly picked for representing the physical effects of the processes but not for directly comparing the sizes.

In Fig. 3a, about 390 nm thick Si was observed on top of the tip of a ~210 nm diameter VACNF, forming a cotton-swab-shaped shell. The largest portion was ~430 nm in diameter near the very end of the CNF tip. The tapered Si shell extended over the whole length of the CNF. The coaxial Si shell below the CNF tip showed a feather-like texture with modulated contrast, different from the uniform Si deposits above the tip. This might be related to the broken graphitic edges along the sidewall of the PECVD-grown VACNFs as observed in our previous studies[25,26] and other literature.[18,20,27] These broken graphitic edges may be critical in forming a good interface between the VACNF core and the Si shell to facilitate fast electron transfer.

Lithium ion intercalation and extraction in "as-grown" VACNF electrodes

The cup-stacking graphitic structure of VACNFs allows Li^+ intercalation into the graphitic layers at the sidewall. The Li^+ transport path across the CNF wall is very short (with D = ~290 nm as illustrated in Fig. S4†), quite different from the long path from the open ends in commonly used seamless carbon nanotubes (CNTs). Indeed, the electrochemical characterization in Fig. S5† illustrated such a phenomenon. A freshly assembled half-cell typically showed the open circuit potential (OCP) of the "as-grown" VACNF anode was ~2.50 to 3.00 V *vs.* Li/Li^+ reference electrode. The CVs measured between 0.001 V and 1.50 V show that Li^+ intercalation starts as the electropotential is below 1.20 V. The first cycle from OCP to 0.001 V involved the formation of a necessary protective layer, *i.e.* the solid electrolyte interphase (SEI), by the decomposition of solvent, salts, and impurities,[28–31] and thus presented a large cathodic current. Subsequent CVs showed smaller but more stable currents. The cathodic current associated with Li^+ intercalation rose slowly as the electrode potential was swept to negative until a sharp cathodic peak appeared at 0.18 V. As the electrode potential was reversed to positive after reaching the low limit at 0.001 V, lithium extraction was observed in the whole range up to 1.50 V, indicated by the continuous anodic current and a broad peak at 1.06 V.

The CV features of VACNF arrays were somewhat different from those of staged intercalation into graphite[31,32] and slow Li^+ diffusion into the hollow channel of CNTs.[33] Li-ion insertion into VACNFs is likely through intercalation between graphitic

layers from the sidewall due to its unique structure. Interestingly, the TEM image in Fig. S3b† indicates that the graphitic stacks in the bamboo-like nodes inside the CNF seem to be disrupted during Li^+ intercalation–extraction cycles, possibly due to a large volume change. Some debris and nanoparticles were left inside CNFs as well as at the exterior surface.

The galvanostatic charge–discharge profiles in Fig. S5b† showed that the Li^+ storage capacity decreased as the power rate was increased from C/2 to C/0.5 (also referred to as "2C"). To make it easier to compare the rates (particularly for those higher than C/1), we use the fractional notation C/0.5 in this report instead of "2C" that is more popularly used in the literature. The Li^+ intercalation and extraction capacities were normalized to the estimated mass of the CNFs ($\sim 1.1 \times 10^{-4}$ g cm^{-2}) that was calculated based on a hollow VACNF structure with the following average parameters: length (3.0 μm), density (1.1×10^9 CNFs per cm^2), outer diameter (147 nm), and hollow inner diameter (49 nm, ~1/3 of the outer diameter). The density of the solid graphitic wall of the VACNFs was assumed to be the same as graphite (2.2 g cm^{-3}).[32] At the normal C/2 rate, the intercalation capacity was 430 mA h g^{-1} and the extraction capacity is 390 mA h g^{-1}, both of which are slightly higher than the theoretical value of 372 mA h g^{-1} for graphite,[33] which may be attributed to SEI formation and the irreversible Li^+ insertion into the hollow compartments inside the VACNFs. But the uncertainty in mass estimation does not allow a firm conclusion at this stage. The extraction capacities were found to be more than 90% of the intercalation values at all power rates and both the intercalation and extraction capacities decreased by ~9% as the power rate increased from C/2 to C/1 and by ~20% from C/1 to C/0.5, comparable to graphite anodes.

Upon charge–discharge cycling, the intercalation capacity was found to slightly drop from 410 mA h g^{-1} to 370 mA h g^{-1} after 20 cycles at the C/1 rate, while the extraction capacity was maintained between 375 and 355 mA h g^{-1}. The overall coulombic efficiency (*i.e.* the ratio of extraction capacity to intercalation capacity) was ~94%, except in the first two cycles due to SEI formation on the CNF surface. The SEI film is known to form readily on carbonaceous anodes during the initial cycles which allows lithium ion diffusion but is electrically insulating, leading to an increase in series resistance.[31] The TEM image (Fig. S3b†) and SEM image (Fig. S6a†) show that a non-uniform thin film was deposited on the CNF surface during charge–discharge cycles. The SEI may actually serve as a sheath to increase the mechanical strength of the VACNFs, preventing them from collapsing into microbundles by the cohesive capillary force of the solvent as observed in the study with other polymer coatings.[34]

Lithium ion insertion and extraction in silicon-coated VACNF core–shell NW electrodes

The most exciting results were obtained with the Si-coated VACNF core–shell NW array as Li-ion battery anodes shown in Fig. 4. The CVs in Fig. 4a present very similar features to those of Si NWs.[9] Compared to the "as-grown" VACNF array, both the cathodic wave for Li^+ insertion and the anodic wave for Li^+ extraction shift to lower values (below ~0.5 and 0.7 V, respectively). The peak current density increases by 10 to 30 times after Si coating and is directly proportional to the scan rate. Clearly, alloy-forming Li^+ insertion into Si is much faster than intercalation into VACNFs that was limited by the slow diffusion of Li^+ between graphitic layers. The cathodic peak at ~0.28 V was not observed in the previous study on pure Si NWs.[9] The three anodic peaks representing the transformation of the Li–Si alloy into amorphous Si are similar to those with Si NWs[35] despite shifting to lower potentials by 100 to 200 mV.

The galvanostatic charge–discharge profiles of a Si-coated VACNF core–shell NW array (Fig. 4b) showed two remarkable features: (1) a high Li^+ insertion (charge) and extraction (discharge) capacity of ~3000 mA h $(g_{Si})^{-1}$ was obtained at the C/2 rate even after 120 cycles; and (2) the Li^+ capacity was nearly the same at the C/2, C/1, and C/0.5 power rates. The total Li^+ storage capacity after Si deposition is about 10 times that of "as-grown" VACNFs even though the low potential limit for the charging cycle was increased from 0.001 V to 0.050 V. As a result, the amount of Li^+ intercalation into the VACNF core was negligible. The specific capacity was calculated by dividing only the mass of Si that was calculated from the measured nominal thickness and a bulk density of 2.33 g cm^{-3}. This method was chosen as an appropriate metric to compare the specific capacity of the Si shell to the theoretical value of bulk Si. For the 3.0 μm long VACNF arrays deposited with a Si of 0.456 μm nominal thickness, the areal mass density of Si coating was $\sim 1.06 \times 10^{-4}$ g cm^{-2}, comparable to that of VACNFs ($\sim 1.1 \times 10^{-4}$ g cm^{-2}). The corresponding coulombic efficiency in Fig. 4b is greater than 99% at all three power rates, much higher than that of the "as-grown" VACNFs.

Both the CVs and charge–discharge measurements indicated that the Li^+ insertion into the Si shell was fast and highly reversible, which are desired for high-performance Li-ion battery anodes. This was further demonstrated with two long cycling tests on two identical samples at different testing conditions: (1) slow asymmetric tests with the C/2 rate for insertion and the C/5 rate for extraction; and (2) the fast symmetric test at the C/1 rate for both insertion and extraction. Both sets of data showed >98% coulombic efficiency over the long cycling except for the initial conditioning cycles (4 cycles in the former and 12 cycles in the latter at varied low rates). In the slow asymmetric tests, the insertion capacity only dropped by 8.3% from 3643 mA h g^{-1} at the 5th cycle to 3341 mA h g^{-1} at the 100th cycle. Even at the fast C/1 charge–discharge rate, the insertion capacity only drops by 11% from 3096 mA h g^{-1} at the 13th cycle to 2752 mA h g^{-1} at the 100th cycle. The difference in the Li^+ capacity between these two sets of data was mostly attributed to the initial conditioning parameters and small sample-to-sample variations. This was indicated by the similar values of insertion–extraction capacity during the first few conditioning cycles in Fig. 4c at C/10 and C/5 rates. The fast rates (C/0.5 for 9th and 10th cycles and C/0.2 for 11th and 12th cycles in sample #2) were found to be harmful and caused an irreversible drop in the capacity. However, the electrode became stabilized after long cycling. As shown in Fig. 4b, the charge–discharge profiles are almost identical at C/2, C/1, and C/0.5

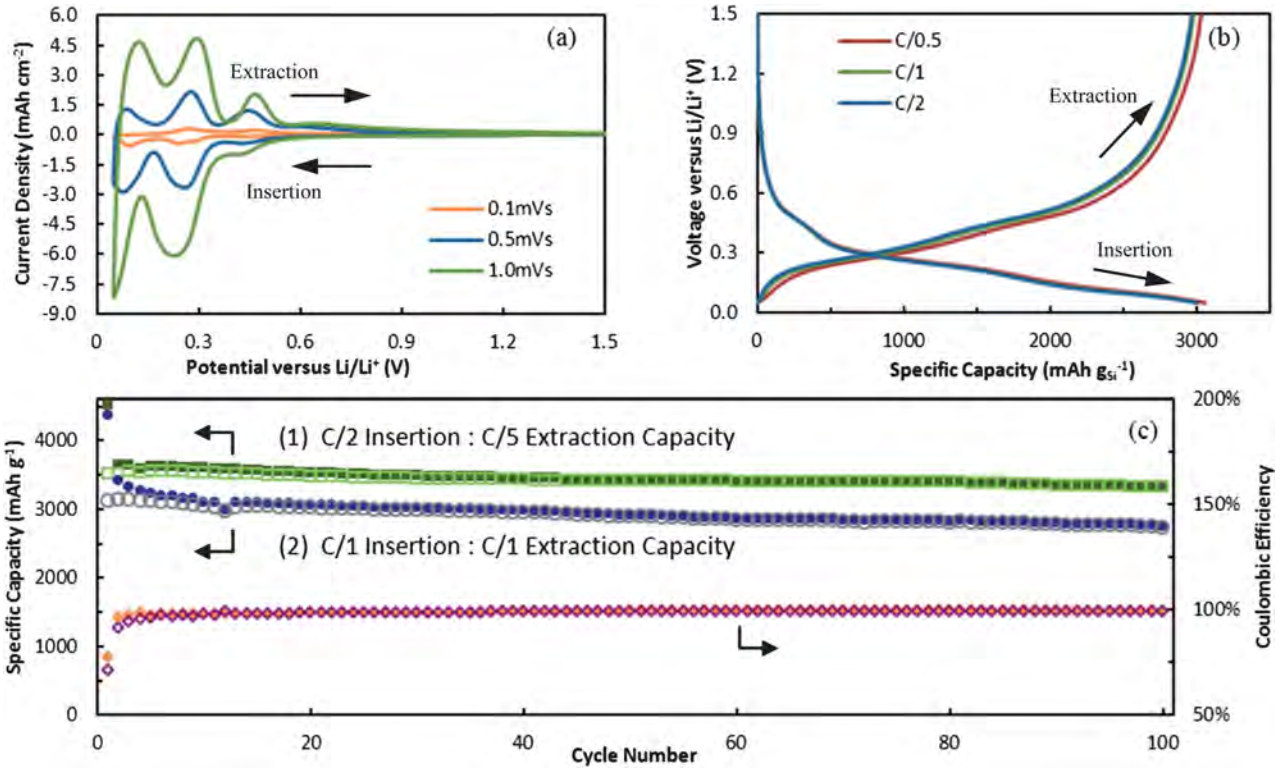

Fig. 4 Characterization of lithium insertion and extraction of Si-coated 3.0 μm long VACNFs at a nominal Si thickness of 0.50 μm. (a) Cyclic voltammograms between 1.5 V and 0.05 V *versus* Li/Li^+ at 0.10, 0.50 and 1.0 mV s^{-1} scan rates. The measurements were made after the sample going through 150 charge–discharge cycles and the data of the second cycle at each scan rate are shown. (b) The galvanostatic charge–discharge profiles at C/0.5, C/1 and C/2 power rates with the sample going through 120 cycles. All profiles were taken from the second cycle at each rate. (c) Insertion and extraction capacities (to the left vertical axis) and coulombic efficiency (to the right vertical axis) of two electrodes *versus* the charge–discharge cycle number. The first electrode was first conditioned with one cycle at the C/10 rate, one cycle at the C/5 rate, and two cycles at the C/2 rate. It was then tested at the C/2 insertion rate and C/5 extraction rate for the rest of the 96 cycles. The filled and open green squares represent the insertion and extraction capacities, respectively. The second electrode was first conditioned with two cycles each at C/10, C/5, C/2, C/1, C/0.5 and C/0.2 rates. It was subsequently tested at the C/1 rate for the next 88 cycles. The insertion and extraction capacities for this electrode are represented by filled and open blue circles, respectively. The columbic efficiencies of both electrodes are represented by filled (1st electrode) and open (2nd electrode) diamonds, which mostly overlap at 99%.

rates, which were measured with sample #1 after going through 120 cycles. To our knowledge, such remarkable cycle stability and high-rate capability are only attainable with ultrathin (<50 nm) Si films.[10]

The specific capacity of the Si shell in the range of 3000 to 3650 mA h g^{-1} is consistent with the highest values of amorphous Si anodes summarized in the comprehensive review by Szczech and Jin.[36] It is remarkable that the entire Si shell in the VACNF–Si core–shell NW array was active for Li^+ insertion and remained nearly 90% of the capacity over 120 cycles, which to our knowledge has not been achieved before except with ultrathin (<50 nm) Si films.[10] The specific capacity obtained in this study is significantly higher than those using other nanostructured Si materials at similar power rates, including ~2500 mA h g^{-1} at the C/2 rate and ~2200 mA h g^{-1} at the C/1 rate with Si NWs,[9] and ~800 mA h g^{-1} at the C/1 rate with randomly oriented carbon nanofiber–Si core–shell NWs.[14] Clearly, the coaxial core–shell NW structure on well-separated VACNFs provides an enhanced charge–discharge rate, nearly full Li^+ storage capacity of Si, and a long cycle life. The more uniform Si shell and better electrical interface with the VACNFs may be the key for the enhanced performance.

As shown in Fig. 4c, an anomalously high insertion capacity (~4500 mA h g^{-1}) was always observed in the initial cycles, which was 20–30% higher than the latter ones. In contrast, the extraction values were relatively stable over all cycles. The extra insertion capacity can be attributed to the combination of three irreversible reactions: (1) the formation of a thin SEI layer (of tens of nanometers);[36–38] (2) reactions of Li with SiO_x presented on the Si surface ($SiO_x + 2xLi \rightarrow Si + xLi_2O$);[17] and (3) the conversion of the starting crystalline Si coating with a higher theoretical capacity (~4200 mA h g^{-1}) into amorphous Si with lower capacity (<3800 mA h g^{-1}).[36] The TEM image (Fig. 3b) and SEM image (Fig. S6b†) showed that a non-uniform SEI might have been deposited on the surface of the Si shell after the charge–discharge cycles. This elastic SEI film likely helped to retain the Si shell on the VACNF surface as it went through the large volume expansion–contraction cycles. The dramatic difference between the SEM images in Fig. S6b and S6c† indicates the large expansion of the Si shell in the lithiated (charged) state as the electrochemical cell was dissembled, although some of the expansion may be due to later oxidation of Li by air. The energy dispersive X-ray spectroscopy (EDS) measurements in Fig. S7† at the tip of a Si-coated VACNF array

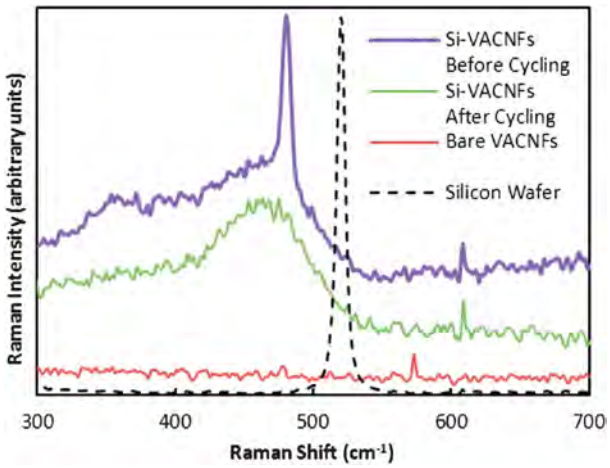

Fig. 5 Raman spectra of a bare VACNF array (red line) and a Si-coated VACNF array before (blue line) and after (green line) charge–discharge cycling in a Li-ion half-cell test compared to the reference using a Si(100) wafer (black dashed line). The measurements were recorded with a Raman microscope with 532 nm laser at 5 mW power.

indicate that the atomic ratio of oxygen to Si was ~0.22 : 1 in the Si shell, which was expected since the samples were stored in the air from a few weeks to several months before the measurements.

The crystalline and amorphous structure of the Si shell was revealed by Raman spectroscopy. As shown in Fig. 5, the pristine Si-coated VACNF array showed multiple broad bands overlapped in the range of 350 to 550 cm^{-1} corresponding to amorphous Si, and a much higher sharp band at 480 cm^{-1} corresponding to nanocrystalline Si.[17,39] After charge–discharge tests, the sharp peak disappeared while the broad bands merged into a single peak at 470 cm^{-1}. The bare VACNF sample did not show any feature in this range. Interestingly, the crystalline Si peak downshifted by ~40 cm^{-1} from that measured with a single-crystalline Si(100) wafer and by ~20 to 30 cm^{-1} from other micro-crystalline Si materials.[17,39] This shift was likely due to the much smaller crystal size and large disorders. The original Si shell likely consisted of nanocrystals embedded in an amorphous matrix associated with the feather-like TEM image in Fig. 3a. After initial cycles, the Si nanocrystals were converted into amorphous Si, consistent with the featureless TEM image after the cycling test (see Fig. 3b). However, the Si shell apparently did not slide along the CNF, in contrast to the large longitudinal expansion (by up to 100%) in pure Si NWs.[9] The volume change of the Si shell during Li^+ insertion was dominated by radial expansion, while the CNF–Si interface remained intact.

The effects of VACNF length and silicon shell thickness

From previous results and discussions, it is clear that the open space between the core–shell NWs is critical for high cycling stability by allowing the Si shell to freely expand/contract. Since an optimum electrode structure depends on both the VACNF length and Si shell thickness, it is always desirable to use longer VACNFs and thicker Si coatings in order to obtain higher total

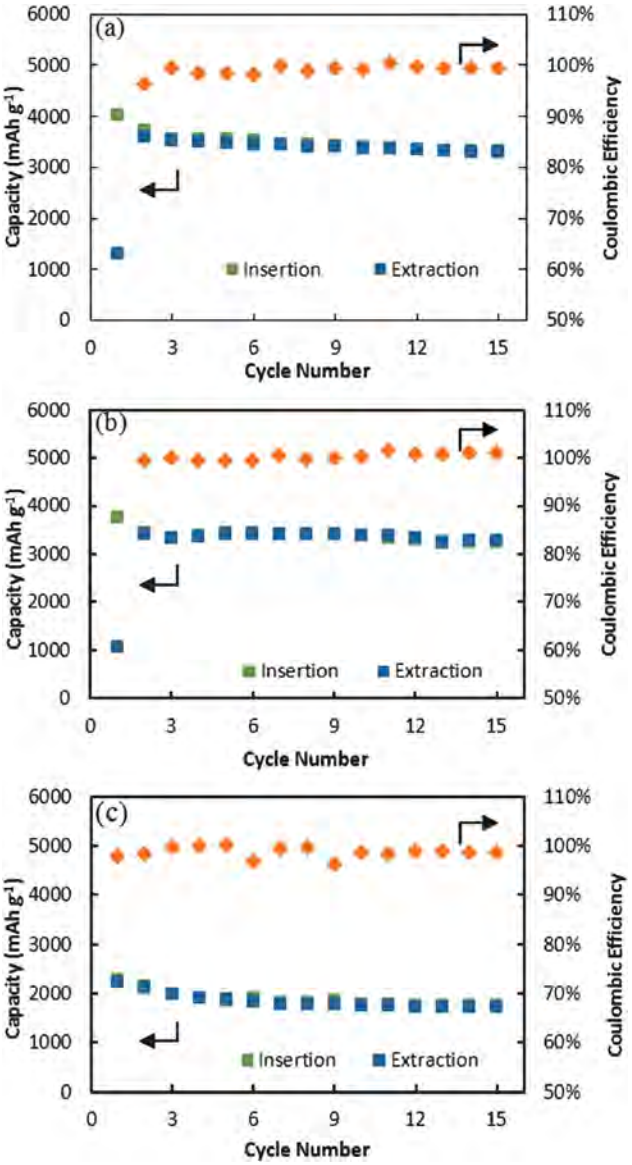

Fig. 6 The lithium insertion and extraction capacities and coulombic efficiency *versus* the cycle number with a 10 μm long VACNF array coated with Si at varied thicknesses. The nominal Si thickness is (a) 0.5 μm, (b) 1.5 μm, and (c) 4.0 μm, respectively, measured *in situ* with a quartz crystal microbalance during sputtering. The samples were first conditioned at the C/10 charge–discharge rate for the first cycle, the C/5 rate for the second cycle, and the C/2 rate for Li^+ insertion but the C/5 rate for Li^+ extraction in the remaining cycles.

Li^+ storage capacity. We have found that longer VACNFs indeed improve the core–shell structure and storage capacity.

Fig. 6 shows the variation of Li^+ insertion–extraction capacities and the coulombic efficiency over 15 charge–discharge cycles with three 10 μm long VACNF samples deposited with Si at a nominal thickness of 0.50, 1.5 and 4.0 μm, respectively. After conditioning at the C/10 rate for the first cycle and the C/5 rate for the second cycle, asymmetric rates (C/2 for insertion and C/5 for extraction) were used in subsequent cycles similar to the measurements of sample #1 in Fig. 4c. This protocol provided nearly 100% coulombic efficiency and minimum degradation.

The specific capacities as high as 3597 mA h g^{-1} and 3416 mA h g^{-1} were obtained with 0.50 and 1.5 μm Si coating, respectively, very similar to that with 0.50 μm Si on 3.0 μm long VACNFs (see Fig. 4c). The capacity remained nearly constant over 15 cycles. However, the electrode with 4.0 μm nominal Si thickness showed a significantly lower specific capacity at only 2221 mA h g^{-1}. This indicates that, with expansion, the Si coatings from adjacent CNFs began to run into each other, limiting them from further expansion. As a result, only a fraction of the silicon coating was active in lithium insertion. The cycle stability was correspondingly worse than the sample with thinner Si coatings.

Interestingly, the same amount of Si (500 nm nominal thickness) on 10 μm VACNF arrays gave nearly the same amount of Li^+ storage capacity (3597 mA h g^{-1}, see Fig. 6a) as that of 3 μm VACNF arrays (3643 mA h g^{-1}, see Fig. 4c), even though the carbon mass is more than 3 times higher. This is very strong experimental evidence that the contribution of VACNFs is negligible in calculating Li^+ storage. It is likely that very little Li^+ ions were intercalated into VACNFs in the Si-coated sample, which is why the core–shell structure was very stable during long charge–discharge cycles.

The variation of the specific Li^+ storage capacity in the three samples correlated well with their structures revealed by the SEM images in Fig. S8.† At 0.50 μm nominal Si thickness, the average tip diameter was found to be ~388 nm on the 10 μm long VACNFs, much smaller than the ~457 nm average diameter on the 3.0 μm long VACNF arrays. The Si shell was thinner but more uniformly spread along the 10 μm long VACNFs. This can be attributed to two reasons: (1) as the same amount of Si was spread over longer VACNFs, the thickness of the Si shells was reduced; and (2) the structure of 10 μm VACNFs differed in some aspects from the 3 μm VACNFs.

It is noted that growing 10 μm VACNFs took 120 min, about six times as long as growing the 3 μm VACNFs. Some Ni catalysts were slowly etched by NH_3 during the long PECVD process, resulting in continuous reduction in the Ni nanoparticle size and leading to the tapered VACNF tip (as shown in Fig. S9†). The CNF length variation also increased in long VACNF arrays. These factors collectively reduced the shadow effects of the VACNF tip. As a result, even at 1.5 μm nominal Si thickness, the VACNF–Si core–shell NWs are well separated from each other. The SEM image of 1.5 μm Si on 10 μm VACNF arrays (Fig. S8b†) is very similar to that of 0.50 μm Si on 3.0 μm VACNF arrays (Fig. 2b). But as the nominal Si thickness was increased to 4.0 μm, the Si shells clearly merged with each other and filled up most of the space between the VACNFs (see Fig. S8c†). This reduced the free space needed to accommodate the volumetric expansion of the Si shell. As a result, the specific Li^+ storage capacity significantly dropped. The VACNF array with thick Si coating behaved somewhat similar to other hybrids of silicon with nanostructured carbon.[14,15,21]

The effect of Si thickness is further illustrated in Fig. 7 which compares the mass-specific capacity (normalized to the total Si mass) and area-specific capacity (normalized to the geometric surface area of the Cu substrate) for lithium insertion with nine 10 μm VACNF samples at the three Si thicknesses. As shown in Fig. 7a, the samples with 0.50 and 1.5 μm nominal Si thicknesses have comparable mass-specific capacities of 3208 ± 343 and 3212 ± 234 mA h g^{-1}, respectively. The samples with a 4.0 μm nominal Si thickness give much lower capacity at 2072 ± 298 mA h g^{-1}. Clearly, the thinner Si coatings are fully activated and provide the maximum Li insertion capacity that amorphous Si could afford. On the other hand, the area-specific capacity in Fig. 7b increases proportionally with the Si thickness from 0.373 ± 0.040 mA h cm^{-2} at 0.50 μm Si to 1.12 ± 0.08 mA h cm^{-2} at 1.5 μm Si but drops off from the linear curve to give 1.93 ± 0.28 mA h cm^{-2} at 4.0 μm nominal Si thickness. Clearly, only a fraction of the extra silicon in the thick Si coating is actively involved in Li storage. The electrochemical results are consistent with the structure shown in SEM images in Fig. S8.†

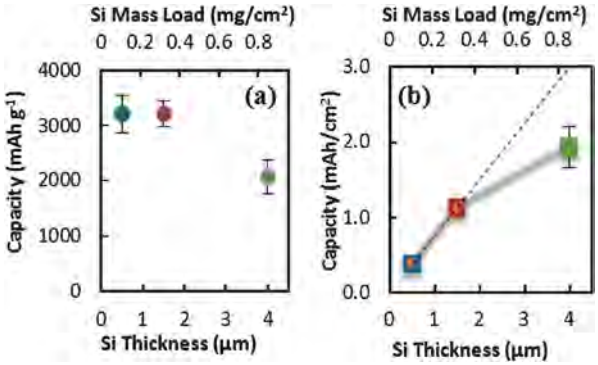

Fig. 7 The specific lithium insertion capacity normalized to (a) the mass of Si coating and (b) the geometric electrode area. The measurements were carried out with 10 μm long VACNF arrays at the C/2 rate for Li^+ insertion (charge) and C/5 for Li^+ extraction (discharge). Both the nominal Si thickness (in μm) and the areal Si mass load (in mg cm^{-2}) on the samples were shown in horizontal axes. A total of 9 samples were measured, with three at each nominal silicon thickness of 0.5, 1.5, and 4.0 μm. The dashed line in panel (b) represents the speculated linear relationship between the area-specific capacity and the nominal Si thickness. The measured capacity drops off from this line at a nominal Si thickness of 4.0 μm.

From this study, it is expected that the optimum structure for this electrode is to coat uniform thin Si shells (~200 to 300 nm radial thickness) on very long VACNFs (30–40 microns) with smaller diameters (~50 nm), and grown on thinner metal foils (10 microns). This remains to be a challenging research topic at this stage. We are currently investigating varying the parameters, including VACNF length, density and silicon coating thickness on low-density VACNF samples, as well as more conformal deposition techniques (such as CVD, atomic layer deposition, and electrochemical deposition) for Si and other Li-ion active materials.

Conclusion

Here, we have demonstrated a high-performance hybrid lithium-ion anode material based on coaxially coated Si shells on VACNF cores. VACNF arrays are not only a good nanostructured template with excellent mechanical robustness but also provide an effective electrical interface with the entire Si shell due to the unique cup-stacking graphitic microstructure. Thick Si layers (equivalent to 1.5 μm nominal thickness on a flat

surface) were deposited onto 10 μm long VACNF arrays, which can still maintain the open vertical core–shell nanowire structure with individual nanowires well separated from each other. This unique hybrid architecture allowed the Si shell to freely expand/contract in the radial direction during Li^+ insertion/extraction. High-performance Li storage with a mass-specific capacity of 3000 to 3650 mA h g^{-1} was obtained even at the C/1 rate. The capacity matched the maximum value that amorphous Si could afford, indicating that the Si shell was fully active. This 3D nanostructured architecture enables effective electrical connection with bulk quantities of Si material while maintaining a short Li^+ insertion–extraction path. As a result, high capacity near the theoretical limit was attained in over 120 charge–discharge cycles and there was little change as the rate was increased 20 times from C/10 to C/0.5 (or 2C). The high capacity at significantly improved power rates and the extraordinary cycle stability make this novel structure a very promising anode material for future high-performance Li-ion batteries. The same core–shell concept may be applied to cathode materials by replacing the Si shell with TiO_2, $LiCoO_2$, $LiNiO_2$, $LiMn_2O_4$, $LiFePO_4$, *etc.* Assembling hybrid structures using the well-defined VACNF array template is a viable approach for energy storage technologies.

Acknowledgements

The work at Kansas State University was supported by NSF grant CMMI-1100830, Kansas Space Grant Consortium, and partially from NSF EPSCoR Award EPS-0903806 (including the matching support from the State of Kansas through Kansas Technology Enterprise Corporation). We would like to thank Dr Lateef U. Syed, Romil Bhandavat, and Prof. Kenneth Klabunde for assistances.

Notes and references

1 D. R. Rolison and L. F. Nazar, *MRS Bull.*, 2011, **36**, 486–493.
2 F. T. Wagner, B. Lakshmanan and M. F. Mathias, *J. Phys. Chem. Lett.*, 2010, **1**, 2204–2219.
3 A. S. Arico, P. Bruce, B. Scrosati, J. M. Tarascon and W. Van Schalkwijk, *Nat. Mater.*, 2005, **4**, 366–377.
4 T. S. Arthur, D. J. Bates, N. Cirigliano, D. C. Johnson, P. Malati, J. M. Mosby, E. Perre, M. T. Rawls, A. L. Prieto and B. Dunn, *MRS Bull.*, 2011, **36**, 523–531.
5 J. W. Long, B. Dunn, D. R. Rolison and H. S. White, *Chem. Rev.*, 2004, **104**, 4463–4492.
6 J. M. Tarascon and M. Armand, *Nature*, 2001, **414**, 359–367.
7 J. Molenda and J. Marzec, *Funct. Mater. Lett.*, 2008, **1**, 91–95.
8 B. A. Boukamp, G. C. Lesh and R. A. Huggins, *J. Electrochem. Soc.*, 1981, **128**, 725–729.
9 C. K. Chan, H. L. Peng, G. Liu, K. McIlwrath, X. F. Zhang, R. A. Huggins and Y. Cui, *Nat. Nanotechnol.*, 2008, **3**, 31–35.
10 S. Ohara, J. Suzuki, K. Sekine and T. Takamura, *J. Power Sources*, 2004, **136**, 303–306.
11 J. P. Maranchi, A. F. Hepp, A. G. Evans, N. T. Nuhfer and P. N. Kumta, *J. Electrochem. Soc.*, 2006, **153**, A1246–A1253.
12 J. P. Maranchi, A. F. Hepp and P. N. Kumta, *Electrochem. Solid-State Lett.*, 2003, **6**, A198–A201.
13 H. Chen, J. Xu, P.-c. Chen, X. Fang, J. Qiu, Y. Fu and C. Zhou, *ACS Nano*, 2011, **5**, 8383–8390.
14 L. F. Cui, Y. Yang, C. M. Hsu and Y. Cui, *Nano Lett.*, 2009, **9**, 3370–3374.
15 P. C. Chen, J. Xu, H. T. Chen and C. W. Zhou, *Nano Res.*, 2011, **4**, 290–296.
16 W. Wang, R. Epur and P. N. Kumta, *Electrochem. Commun.*, 2011, **13**, 429–432.
17 J. Qu, H. Q. Li, J. J. Henry, S. K. Martha, N. J. Dudney, H. B. Xu, M. F. Chi, M. J. Lance, S. M. Mahurin, T. M. Besmann and S. Dai, *J. Power Sources*, 2012, **198**, 312–317.
18 A. V. Melechko, V. I. Merkulov, T. E. McKnight, M. A. Guillorn, K. L. Klein, D. H. Lowndes and M. L. Simpson, *J. Appl. Phys.*, 2005, **97**, 41301.
19 M. Meyyappan, L. Delzeit, A. Cassell and D. Hash, *Plasma Sources Sci. Technol.*, 2003, **12**, 205–216.
20 Z. F. Ren, Z. P. Huang, J. W. Xu, J. H. Wang, P. Bush, M. P. Siegal and P. N. Provencio, *Science*, 1998, **282**, 1105–1107.
21 W. Wang and P. N. Kumta, *ACS Nano*, 2010, **4**, 2233–2241.
22 B. A. Cruden, A. M. Cassell, Q. Ye and M. Meyyappan, *J. Appl. Phys.*, 2003, **94**, 4070–4078.
23 J. Liu, J. Essner and J. Li, *Chem. Mater.*, 2010, **22**, 5022–5030.
24 Q. Ngo, T. Yamada, M. Suzuki, Y. Ominami, A. M. Cassell, J. Li, M. Meyyappan and C. Y. Yang, *IEEE Transactions on Nanotechnology*, 2007, **6**, 688–695.
25 Q. Ngo, A. M. Cassell, A. J. Austin, J. Li, S. Krishnan, M. Meyyappan and C. Y. Yang, *IEEE Electron Device Lett.*, 2006, **27**, 221–224.
26 L. U. Syed, J. Liu, A. M. Prior, D. H. Hua and J. Li, *Electroanalysis*, 2011, **23**, 1709–1717.
27 E. C. Landis and R. J. Hamers, *J. Phys. Chem. C*, 2008, **112**, 16910–16918.
28 D. Aurbach, M. D. Levi, E. Levi and A. Schechter, *J. Phys. Chem. B*, 1997, **101**, 2195–2206.
29 D. Aurbach, Y. Talyosef, B. Markovsky, E. Markevich, E. Zinigrad, L. Asraf, J. S. Gnanaraj and H. J. Kim, *Electrochim. Acta*, 2004, **50**, 247–254.
30 G. K. Simon and T. Goswami, *Metall. Mater. Trans. A*, 2011, **42**, 231–238.
31 Y. W. Perla and B. Balbuena, *Lithium-Ion Batteries: Solid-Electrolyte Interphase*, Imperial College Press, River Edge, NJ, 2004.
32 *Crc Handbook of Chemistry and Physics*, ed. D. R. Lide, CRC Press, New York, 2004.
33 M. Winter, K.-C. Moeller and J. O. Besenhard, in *Lithium Batteries: Science and Technology*, ed. G.-A. Nazri and G. Pistoia, Kluwer Academic Publishers, Boston, 2004, pp. 144–194.
34 T. B. Nguyen-Vu, H. Chen, A. Cassell, R. Andrews, M. Meyyappan and J. Li, *Small*, 2006, **2**, 89–94.

35 W. Wan, Q. Zhang, Y. Cui and E. Wang, *J. Phys.: Condens. Matter*, 2010, **22**, 415501.
36 J. R. Szczech and S. Jin, *Energy Environ. Sci.*, 2011, **4**, 56–72.
37 V. Etacheri, R. Marom, R. Elazari, G. Salitra and D. Aurbach, *Energy Environ. Sci.*, 2011, **4**, 3243–3262.
38 D. Aurbach, *Advances in Lithium-ion Batteries*, ed. W. Schalkwijk and B. Scrosati, Kluwer Academic Publishers, New York, 2002, pp. 7–77.
39 I. Abdulhalim, R. Beserman and R. Weil, *Phys. Rev. B: Condens. Matter Mater. Phys.*, 1989, **39**, 1081–1091.